# EVALUATION OF NANOCRYSTALLINE MATERIALS, AMORPHOUS ALLOYS AND FERRITES FOR REPETITIVE-MAGNETIC PULSE COMPRESSION APPLICATIONS[†]

**Russell Burdt, Kenneth F. McDonald, Randy D. Curry, Brett Huhman**
*University of Missouri-Columbia*
*Department of Electrical and Computer Engineering*
*Columbia, Missouri 65211*

**Paul Melcher, Richard Ness, Chaofeng Huang**
*Cymer Inc.*
*17075 Thornmint Court*
*San Diego, California 92127*

*Abstract*

Recent advances in nanocrystalline magnetic materials and core insulation techniques are believed to be superior to the current magnetic cores that are employed as saturable switches in solid-state, repetitive magnetic pulse compressors. Accordingly, a magnetic pulse compressor test stand has been constructed at the University of Missouri-Columbia (UMC) to evaluate the switching properties of candidate magnetic materials and insulation schemes that cover the wide parameter space requisite to magnetic modulators. Experimental measurements were utilized to analyze and compare a wide variety of magnetic materials consisting of nanocrystalline cores, amorphous metal alloys and ferrites. The dependence of the insulating material and the core construction techniques, *e.g.*, type and thickness of the insulation and ferromagnetic material were included in a model along with the magnetic core loss measurements. An advanced figure of merit was utilized to down-select the cores for a particular application based on the measurements and the UMC database. Final test results were analyzed to determine which core material had the best switching properties for a specific operational regime.

The test stand, data acquisition equipment and methods, data processing, magnetic core materials under examination and final test results are discussed.

## I. INTRODUTION

Evolving applications for Ultraviolet (UV) excimer lasers demand pulsed power drivers that are highly efficient and highly reliable [1,2]. Consequently, there is an ever-increasing need for high peak power pulse compressors that operate at high repetition rates [3]. The high peak power requirement mandates a voltage step-up transformer and numerous temporal compression stages to allow the first stage to operate within the limits of economical solid-state switches. Moreover, the choice of saturable magnetic switch systems is even more crucial because low pulse energy, high rep-rate operation is quite sensitive to switching losses. Optimization of a pulse compressor requires that different magnetic materials be employed in the various stages, according to the volt-second product, the magnetic flux density inherent to the magnetic switch and the 1-cos(ωt) magnetization time inherent to the particular compression section.

The optimal selection of magnetic switches for each compression stage is further complicated by the recent availability of new magnetic materials, insulation schemes and the fabrication/annealing procedures. Emerging magnetic materials are now becoming available because of recent progress in the development of nanocrystalline magnetic materials [4, 5, 6]. It is important to understand the loss properties of these emerging magnetic materials and also to compare their performance characteristics to conventional materials.

## II. UMC TEST STAND

A magnetic pulse compressor test stand was designed and built at UMC to evaluate the switching properties of candidate magnetic materials and insulation schemes. The test stand is able to generate 1-cos(ωt) waveforms and operate at modest repetition rates. A schematic of the test stand is shown in Figure 1.

[†] Work supported by Cymer Inc.

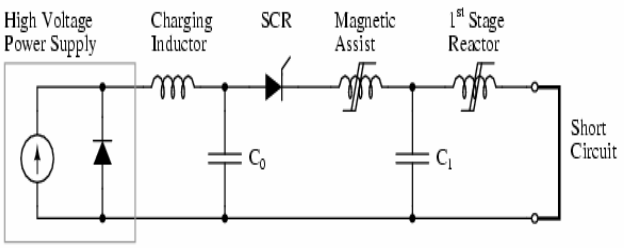


**Figure 1.** Magnetic pulse compressor test stand

The high voltage power supply is capable of charging $C_0$ over a wide range of voltages. Once $C_0$ is charged, the SCR is fired by means of an external trigger pulse, creating a C-L-C topology that generates a 1-cos(ωt) waveform across $C_1$. Once the magnetic assist core saturates, it appears in the circuit as a small saturated inductance with low impedance and the voltage on $C_1$ begins to rise rapidly. The magnetic flux density of the core under test (1st stage reactor) exceeds the saturation limit and then saturates. During this process, the voltage across the core and the current in the circuit are measured and later utilized to generate the B-H curve and quantify the energy losses. The cores are reset with a DC reverse bias current.

## III. DATA ACQUISTION METHODS

The measurements necessary to plot the B-H curve and characterize the losses of a magnetic core include the physical properties of the core, the voltage across the core and the current in the circuit. For the UMC test stand the current in the circuit was measured with a wide-band Pearson Current Monitor and the voltage across the core was directly measured with a Tektronix self-attenuating differential voltage probe. A B-Dot probe was positioned close to the core under test in order to accurately determine the commencement of the current surge. Uncorrelated 'digital' noise was reduced by recording the average of 256 pulse events on a digital oscilloscope.

Data sets were acquired for each magnetic core over a wide range of capacitor charge voltages that commenced at the minimum voltage necessary for core saturation, usually about 100 volts, and increased in 100-volt increments to a maximum of approximately 1000 volts. As a result of varying the charge voltage, saturation times of approximately 2.5 to 7.0 μs were obtained. Modest repetition rates of 5-10 hertz were utilized in order to reduce magnetic core heating during testing.

## IV. DATA ANALYSIS METHODS

A computer program was written in the MatLab language with inputs consisting of the three measured quantities (current, voltage and B-dot) and the physical parameters of the core. The program was responsible for plotting the B-H curve, determining the time to initial saturation, calculating the energy losses and loss factor over the first half cycle of data and a correlation of these parameters with the packing factor, defined as the ratio of the volume of magnetic material to the total core volume. In plotting the B-H curves, the program utilized equations describing the magnetic flux density and the magnetic field strength for a magnetic core, written as

$$B(t) = \left(-1/NA_m\right)\int v(t)dt \qquad (1)$$

$$H(t) = Ni(t)/l_p \qquad (2)$$

where B(t) is the magnetic flux density, N is the number of turns, $A_m$ is the core cross-sectional area, v(t) is the voltage across the core, i(t) is the current in the circuit, and $l_p$ is the magnetic path length into the core.

Throughout the literature on ferromagnetic cores, many definitions exist for the initial time to saturation. For the experiments discussed, UMC and Cymer Inc. investigators down-selected the following definition: the time period commencing at the start of the current surge (50% of the peak value measured by the B-dot probe) and ending when the voltage across the core reached its first peak value (voltage collapse). Figure 2 represents a sample data set on a time scale slightly larger than the saturation time which graphically represents the saturation time definition.

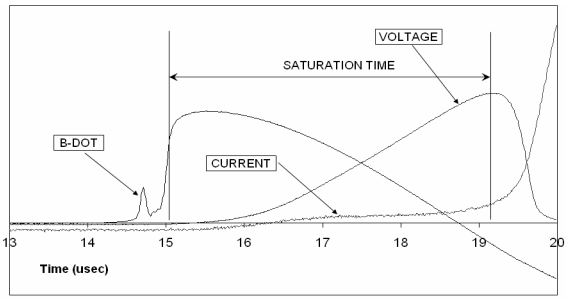


**Figure 2.** Sample data set representing the saturation time definition

The energy loss was calculated as the integral of the voltage-current product with respect to time. The integration interval was taken over the first half cycle of data, from the commencement of the current surge to the first zero of the current waveform.

In order to make material recommendations based on the data, it was necessary to utilize an appropriate comparability parameter. Extensive research into the literature on ferromagnetic cores resulted in the selection of a figure of merit known as the loss factor. This figure of merit was originally defined by Greenwood, Gowar and Bird and is defined as the ratio of the energy loss per unit volume to the square of the available change in flux density [7]. In equation form, the loss factor is written as

$$L_F = \frac{E_{loss}}{V_{eff}(\Delta B)^2} \qquad (3)$$

where $L_F$ is the loss factor, $E_{loss}$ is the first half cycle energy loss, $V_{eff}$ is the measured core volume multiplied by the packing factor and $\Delta B$ is the available change in flux density.

## V. MAGNETIC CORE MATERIALS UNDER EXAMINATION

The different magnetic core materials examined at UMC include Nickel-Iron, Ferrite, Metglas, Finemet and Vitroperm. The fabrication methods and inherent magnetic properties of the nanocrystalline materials will be discussed and sample B-H curves will be presented for Finemet and Vitroperm magnetic cores. A similar discussion for the other types of magnetic cores examined will not be provided as numerous papers already discuss the magnetic properties inherent to Nickel-Iron [8], Ferrite [9] and Metglas magnetic cores [10].

The unique combination of low losses, high permeability, near zero magnetostriction and high saturation magnetization in a magnetic material was first produced by crystallization of an amorphous Fe-Si-B alloy with small additions of Cu and Nb [11]. This new class of iron-based alloys consists of an ultrafine microstructure with grain sizes of 10-15 nm which are known as nanocrystalline magnetic materials. Commercial grades of these alloys are currently available under the trade names Finemet, produced by Hitachi Metals, Ltd. in Japan and Vitroperm, produced by Vacuumschmelze GmbH in Germany. These alloys are of the composition $Fe_{\sim 74}Cu_1Nb_3Si_{13\text{-}16}B_{6\text{-}9}$ with a typical saturation flux density of $B_S$=1.2-1.3 T and an initial unsaturated permeability of $\mu_i=150x10^3$ [11]. The saturation induction and permeability values offered by nanocrystalline magnetic materials have been proven to be higher than other popular alloy compositions such as the permalloys, Sendusts, manganese-zinc ferrites and amorphous cobalt-based alloys. Sample B-H curves for Finemet and Vitroperm magnetic cores at a similar saturation time are shown in Figures 3 and 4, respectively.

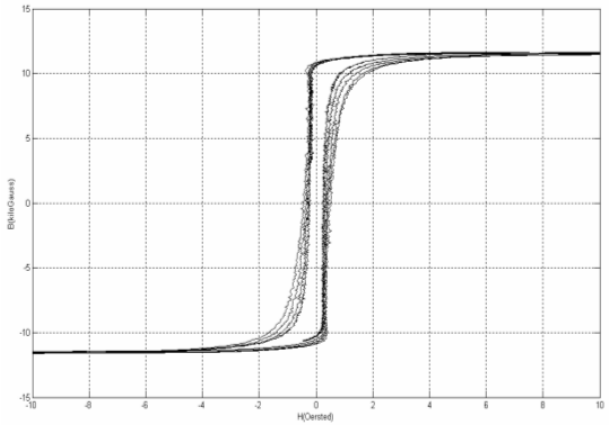

**Figure 3.** BH curve for a Finemet magnetic core

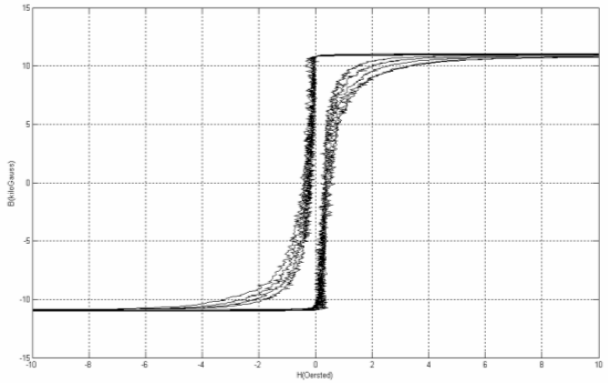

**Figure 4.** BH curve for a Vitroperm magnetic core

## VI. TEST RESULTS

In order to make core-to-core comparisons amongst the wide variety of magnetic materials examined in these experiments, various comparison charts will be employed and material recommendations will be made based on a material's loss factor at a specific saturation time. Comparison charts will be presented for all of the Metglas, Ferrite and Ni:Fe magnetic cores that were examined. Results for the Finemet and Vitroperm magnetic cores will be presented in arbitrary units as the test results for these two materials remain proprietary.

### *A. The Metglas Magnetic Core Comparison*

Metglas pulsed power cores are used in high voltage, high power applications requiring short, narrow pulses at high rep rate. Five different Metglas cores were examined: 2605S3A (iron-based; high permeability), 2605SA1 (iron-based; extremely low core loss), 2714A (cobalt-based; ultra-high permeability), 2605SC (iron-based; square-loop high saturation induction) and 2605CO (iron-based; highest saturation induction).

A loss factor vs. saturation time graph comparing the different Metglas materials is shown in Figure 5 and a loss factor comparison chart at a fixed saturation time of 4.6 μs is shown in Table 1.

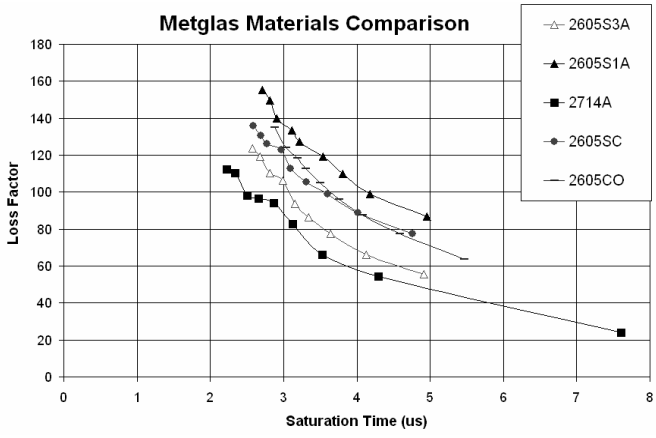


**Figure 5.** Metglas materials comparison

**Table 1.** Metglas materials comparison at 4.6 µs

| Order of Performance (Best to Worst) | Loss Factor (Approximate) | % Increase from Best Performer |
|---|---|---|
| 2714A | 51 | 0 |
| 2605S3A | 60 | 18 |
| 2605CO | 77 | 51 |
| 2605SC | 80 | 57 |
| 2605S1A | 92 | 80 |

The Metglas alloy 2714A had the lowest loss factor of the five Metglas cores that were examined. One factor responsible for this result is that the 2714A alloy is a cobalt-based alloy as opposed to being an iron-based alloy, as are the remaining Metglas cores.

### *B. The Ni-Fe and Ferrite Magnetic Core Comparison*

Six different 50:50 Ni-Fe magnetic cores were examined to determine the effects of varying material thicknesses and insulation properties on the loss factor. Figure 6 shows a loss factor vs. saturation time graph of four 50:50 Ni:Fe cores with identical material thickness but varying insulation properties and from different manufacturers. Figure 7 shows a loss factor vs. saturation time graph of three 50:50 Ni-Fe cores with varying material thickness but with identical insulation properties.

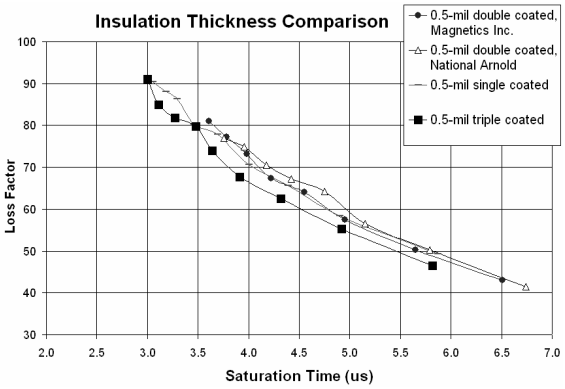


**Figure 6.** 50:50 Ni-Fe insulation thickness comparison

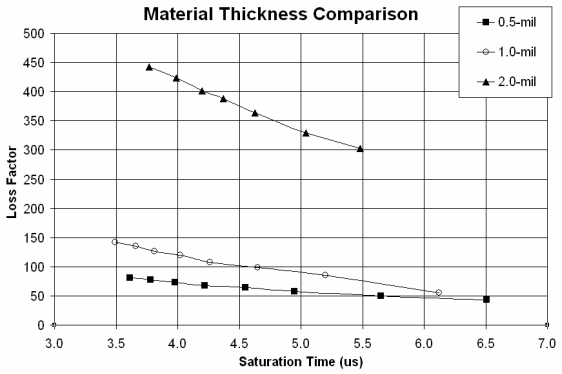


**Figure 7**. 50:50 Ni-Fe material thickness comparison

In Figure 6 the loss factors for the four different cores are within 10% of each other, implying that the insulation properties of a magnetic core have little to no effect on the loss factor. Figure 7 shows that the loss factor for the core with 1.0-mil material thickness is approximately 70% greater than the core with 0.5-mil material thickness and the core with 2.0-mil material thickness has a loss factor approximately 500% greater than the core with 0.5-mil material thickness. This implies that a varying material thickness has a significant impact on the loss factor and a thinner material thickness is desired. This effect is due to reduced eddy current losses in thinner materials.

Two 80:20 Ni-Fe magnetic cores with varying material thickness of 0.45-mil and 0.50-mil and one ferrite magnetic core are compared in Figure 7. The ferrite core was a moderate frequency ferrite designed to meet the requirements of the 0.5 – 30 MHz range, fabricated of CN-20 and manufactured by Ceramic Magnetics, Inc.

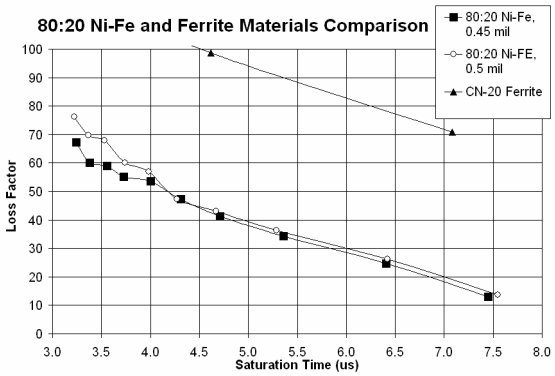


**Figure 8.** 80:20 Ni-Fe and ferrite materials comparison

Figure 8 shows that the two 80:20 Ni-Fe magnetic cores are quantitatively similar in their loss factor vs. saturation time graphs, while the ferrite core has significantly higher losses than both of the 80:20 Ni-Fe cores. Further analysis not presented in this paper indicated that the ferrite core had significantly higher losses than all of the other cores examined in this study. A closer analysis of the 80:20 Ni-Fe magnetic cores is shown in Table 2.

**Table 2.** 80:20 Ni-Fe and Ferrite materials comparison at 4.0µs

| Order of Performance (Best to Worst) | Loss Factor (Approximate) | % Increase from Best Performer |
|---|---|---|
| 80:20 Ni-Fe, 0.45-mil | 54 | 0 |
| 80:20 Ni-Fe, 0.50-mil | 56 | 4 |

Table 2 shows that the 80:20 Ni-Fe magnetic core with 0.50-mil material thickness had a loss factor approximately 4% greater than the core with 0.45-mil material thickness. This result agrees with what was measured in the case of the 50:50 Ni-Fe magnetic core comparison – a varying material thickness has an impact on the loss factor and a thinner material thickness results in a lower loss factor, as would be expected.

### *C. The Finemet Magnetic Core Comparison*

Five different Finemet magnetic cores were examined and will be discussed using arbitrary names as the final test results remain proprietary. Cores A and B were composed of the same magnetic alloy with different dimensional parameters. Cores A, B, and C were designed to have near zero magnetostriction on the order of $10^{-6}$. Cores D and E were designed with a high $\Delta B$, for low core loss operation. The test results for the Finemet magnetic cores presented in Figure 9 are in arbitrary units, as the results remain proprietary.

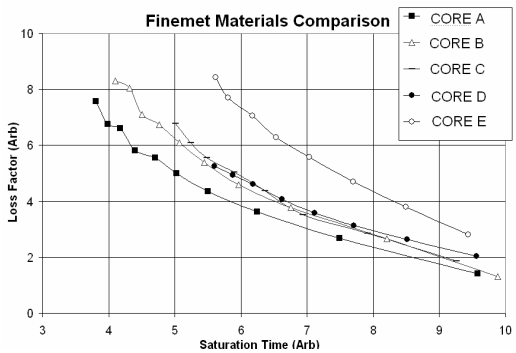


**Figure 9.** The Finemet materials comparison

An analysis of Figure 9 shows that for this particular parameter space core A was the top performing magnetic core in the group. The figure also shows that four of the five Finemet magnetic cores examined had loss factors within 30% of each other.

### *D. The Vitroperm Magnetic Core Comparison*

Two different Vitroperm magnetic cores were examined and will be discussed using arbitrary names as the final test results remain proprietary. First, core A was designed with a high remanence ratio (low $\Delta B_{rs}$, high squareness) for use in efficient magnetic amplifiers. Core B was designed with a high saturation induction and high permeability for use in high frequency applications. The test results for the Vitroperm magnetic cores presented in Figure 10 are in arbitrary units, as the results remain proprietary.

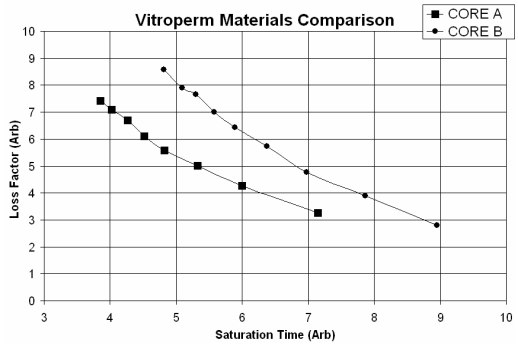


**Figure 10.** The Vitroperm materials comparison

For the parameter space of these experiments the two Vitroperm cores produced loss factor vs. saturation time curves that were similar in shape, but, the B material had a loss factor approximately 50% higher than the A material.

## VII. SUMMARY

A magnetic pulse compressor switch test stand was designed and built at UMC that is capable of generating 1-cos ($\omega t$) waveforms with a variable charge voltage. The test bed rep-rate was variable, but was kept in the 5-10 hertz range in order to reduce magnetic core heating during testing. Data sets were collected and analyzed for a wide variety of magnetic materials consisting of Nickel-Iron, Ferrite, Metglas, Finemet and Vitroperm. Future work will include faster saturation times, impulse *vs.* 1-cos($\omega t$) waveforms and thermal considerations.

## VIII. REFERENCES


[1] R. Ness, P. Melcher, B. Smith, W. Partlo and D. Birx, "Performance Characterization for an Excimer Laser Solid-State Pulsed Power Module (SSPPM) After 20B Shots," IEEE Transactions on Plasma Science, Vol. 28, No .5, October 2000.

[2] P. Melcher, D. Johns, R. Ness, and W. Partlo, "Lifetime and Reliability Data of Commercial Excimer Laser Power Systems Modules," Cymer Inc. San Diego, CA 92127

[3] W. Partlo, R. Sandstrom, I. Fornenkov, and P. Das, "A low cost of ownership Krf excimer laser using a novel pulse power and chamber configuration, Proc. SPIE, Vol. 2440, pp. 90-100, 1995

[4] C. Strowitzki, A. Gortler, M. Baumann, "Losses in Magnetic Switches", Tuilaser AG, Industriestr, 15, Bavaria, Germany

[5] R. Wood and R. Lathlaen, "Exciting New Coatings for Amorphous Glass Pulse Cores," National-Arnold Magnetics, Adelanto, California

[6] C.H. Smith, B.N. Turman, H.C. Harjes, "Insulations for Metallic Glasses in Pulse Power Systems", 19th Power Modulator Symposium, June 28, 1990, San Diego CA

[7] M. Greenwood, J. Gowar, and B.M. Bird, "A Comparability Parameter for Amorphous Magnetic Materials", University of Bristol, Bristol England

[8] S. Winter, R. Kuenning, G. Berg, "Pulse Properties of Large 50-50 Ni-Fe Tape Cores," IEEE Transactions on Magnetics, Vol. 6, Issue 1, March 1970

[9] J. Dolan, H. Bolton, "Field Phenomena in Metglas and Ferrite Magnetic Switches," Proc. 8th IEEE Int'l Pulsed Power Conf., 1991.

[10] Smith, C.H., and Barberi, L., "Dynamic Magnetization of Metallic Glasses," Proc 5th IEEE Int'l Pulsed Power Conf., 1985.

[11] Giselher Herzer, "Nanocrystalline Soft Magnetic Alloys." Handbook of Magnetic Materials, Vol. 10, Ch. 3, Ed. K.H.J. Buschow, 1997, Elsevier